

$^{12}\text{CO } J = 1 - 0$ synthesis images of a dense torus in M 2-9

J. Zweigle¹, R. Neri¹, R. Bachiller², V. Bujarrabal², and M. Grewing¹

¹ Institut de Radio Astronomie Millimétrique (IRAM), 300 Rue de la Piscine, F-38406 Saint Martin d'Hères, France

² Observatorio Astronómico Nacional (I.G.N), Apartado 1143, E-28800 Alcalá de Henares, Madrid, Spain

Received 17 January 1997 / Accepted 18 February 1997

Abstract. We have mapped the $^{12}\text{CO } J = 1 - 0$ emission in the bipolar planetary nebula M 2-9 using the IRAM interferometer. From the maps we were able to investigate in detail the morphology and the kinematics of the molecular gas. The data are best explained by assuming that the molecular gas is concentrated in an expanding, clumpy torus.

The torus, which surrounds the nucleus of M 2-9, has a mean diameter of about $6''$. Its symmetry axis is tilted by 17° with respect to the plane of the sky. The de-projected expansion velocity is 7 km s^{-1} , and its kinematical age is about 2100 years assuming a distance of 1 kpc. The lower limit for the total mass of the molecular gas is estimated to be $9 \cdot 10^{-3} M_\odot$, i.e. at least comparable to the ionized mass in the nebula.

Key words: planetary nebulae: general – planetary nebulae: M 2-9 – radio lines: ISM – stars: mass loss

1. Introduction

M 2-9, the Butterfly nebula, is the prototype of bipolar planetary nebulae (PNe). This object has been used in most theoretical studies addressing the possible relationship between nebular bipolarity and binarity of its nucleus. This is one of the major long standing problems towards the understanding of post-AGB evolution. M 2-9 shows four nebular components: a compact central region, also called core or nucleus, two prominent narrow, open lobes extending north-south to $\pm 20''$, several low ionization knots concentrated along the eastern edges of the lobes and two outer loops, which reach out to $58''$ north and south. Aspin et al. (1988) concluded from near infrared color images, that the core is surrounded by a dense disk of dust having a diameter of about $14''$, which is responsible for the bipolar shape of the nebula.

The complex nature of M 2-9 has intrigued astronomers since its discovery by Minkowski (1947). M 2-9 has been classified as a planetary nebula based on morphological criteria and the position of its central star in the H-R diagram. However, M 2-9 may have an evolutionary history distinct from other planetary

nebulae (PNe). Allen and Swings (1972) placed M 2-9 in the regime of young PNe or symbiotic stars. Observations in different ranges of wavelengths showed that M 2-9 is an object in the early stage of becoming a PN (e.g. Swings & Andrillat 1979, Feibelman 1984). Morris (1981) regarded M 2-9 as an object in a transitional stage between bipolar nebulae and ring-shaped PNe containing a binary nucleus. Balick (1989) noted, that the nucleus of M 2-9 shares many characteristics with very close mass-transfer binary systems. Bachiller et al. (1988, 1990) predicted from their single-dish CO observations the presence of a molecular ring with a diameter less than $10''$ and corroborated the idea that M 2-9 is actually a young planetary nebula. However the angular resolution of their observations was close to the dimensions of the putative ring preventing the study of its characteristics. In this paper we present interferometric observations that confirm the presence of such a molecular ring and reveal its kinematical structure with great detail.

2. Observations

Observations of M 2-9 in the $^{12}\text{CO } J = 1 - 0$ line and in the continuum at a frequency of 115 GHz, were carried out using the IRAM interferometer (Guilloteau et al. 1992) located on the Plateau de Bure, France, in February and March 1995. At that time, the array consisted of four antennas each 15m in diameter, equipped with SIS heterodyne receivers. The observations were done using three different configurations of the array. The effective velocity resolution at the frequency of the CO transition is 0.8 km s^{-1} and the continuum observations cover 360 MHz.

The RF passband and amplitude were calibrated using NRAO 530 (flux 9.5 Jy) and 3C 273 (flux 15.3 Jy). Phase calibration was performed by observing, every 20 minutes, 1741-038, 1749+096 and NRAO 530. The uv data were Fourier transformed and then CLEANed using the Clark algorithm. Due to the southern declination of M 2-9 sidelobes are found in the Dirty beam at a level of -7.2 dB at $\pm 8''$ in the north-south direction. For image restoration, we adopted a Gaussian clean beam of $4.8'' \times 3.1''$ at a position angle of 13° .

A comparison of a synthetic spectrum, which has been calculated by convolving the observed total CO-emission with a Gaussian beam of $21''$, with the $^{12}\text{CO } J = 1 - 0$ spectrum from

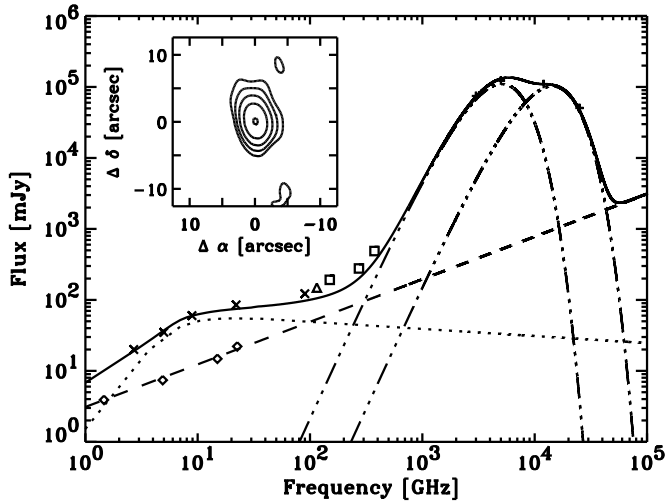


Fig. 1. The continuum flux at 115 GHz observed with the IRAM interferometer (\triangle) compared to single-dish radio (\times , Purton et al. 1982), VLA (\diamond , Kwok et al. 1985), millimetre and submillimetre (\square , Hoare et al. 1992) and IRAS observations ($+$, Phillips and Mampaso 1988). For comparison different emission components are shown: the extrapolated stellar wind component (long dashed) from the VLA observations, the free-free emission of a homogeneous HII-region (dotted) and two modified black-bodies ($T = 55$ K and $T = 155$ K, respectively) for the warm dust emission (dashed-dotted). The solid line is the sum of these contributions. In the upper left corner the spatial distribution of the continuum emission at 115 GHz is inserted (contours at 8 (3σ), 16 , 32 , 64 , and 125 mJy beam $^{-1}$). The spatial units are offsets in arcseconds with respect to the assumed position of the central star.

Bachiller et al. (1988) observed with the IRAM 30m telescope shows that both spectra are compatible within the calibration uncertainties. We conclude therefore that no flux is lost in our interferometric observations.

It is also important to note the possibility that the H 38 α recombination line emission may contribute to the observed CO $J=1-0$ emission in view of the fact that the frequencies of these lines are separated by only 3 MHz. We can, however, rule out this possibility for two reasons: (a) the observed line emission region and the continuum region from which H 38 α emission is supposed to originate, are spatially well separated (see Figs. 1 and 3), (b) the measured systemic velocity in the local standard of rest agrees perfectly with the value given by Bachiller et al. (1990) from their CO $J=2-1$ observations.

3. Results and discussion

3.1. Continuum

The continuum map (see Fig. 1) shows that the continuum emission at 115 GHz comes only from the central region of M 2-9. The continuum flux and the size of the emitting region were determined by Gaussian fits to the measured visibilities and found to be ~ 150 mJy and $2.2'' \times 1.1''$ (north-south oriented), respectively.

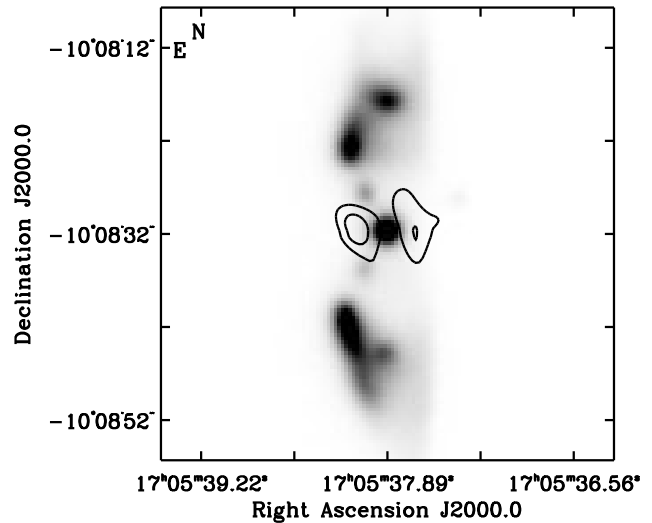


Fig. 2. Comparison of the observed CO emission at the systemic velocity of $v_{\text{SYS}} = 80.2$ km s $^{-1}$ (contours: 125 and 250 mJy beam $^{-1}$) with a CCD image of M 2-9 (grey scale) taken in the [NII] emission line by Balick (1987). In contrast to Fig. 3 the channel width of the CO map used here is only 0.8 km s $^{-1}$.

In Fig. 1 we present a compilation of the continuum flux values observed in a frequency range covering five orders of magnitude. Due to the obvious discrepancy between the WSRT measurements of Kwok et al. (1985) and the VLA data of Zijlstra et al. (1989) we did not take into account both observations. The high flux observed at 115 GHz indicates that the stellar wind component (Kwok et al. 1985) may still significantly contribute to the millimetre flux. The excess flux of about 45 mJy above that expected from the sum of the free-free radiation from ionized gas, the stellar wind component and the emission of warm dust can be very likely attributed to cold dust in the object. However, it is also possible that high-density structure in the stellar wind causes a steepening of the flux density spectral index of the core (at centimetre wavelengths close to 0.6) at millimetre wavelengths. Note that the center of the $^{12}\text{CO } J=1-0$ line emission is shifted in right ascension by $(0.5 \pm 0.3)''$ with respect to the center of the continuum emission ($\alpha_{\text{J2000}} = 17^{\text{h}}05^{\text{m}}37.89^{\text{s}}$, $\delta_{\text{J2000}} = -10^{\circ}08'32.3''$). This may be related to the suspected binarity of the M 2-9 nucleus.

3.2. Morphology and kinematics of the molecular gas

We show in Fig. 2 a grey scale image of M 2-9 taken in the [NII] emission line by Balick (1987), on which the observed CO $J=1-0$ map at the systemic velocity of $v_{\text{SYS}} = 80.2$ km s $^{-1}$ is superimposed as a contour plot. The CO emission shows two maxima on both sides west and east of the nucleus and suggests that the molecular gas is concentrated in a torus which is encircling the core of M 2-9. As we will discuss below, the kinematical structure confirms this first impression.

In order to investigate the kinematical structure of M 2-9 we present in Fig. 3 maps of the CO $J=1-0$ intensity separated by

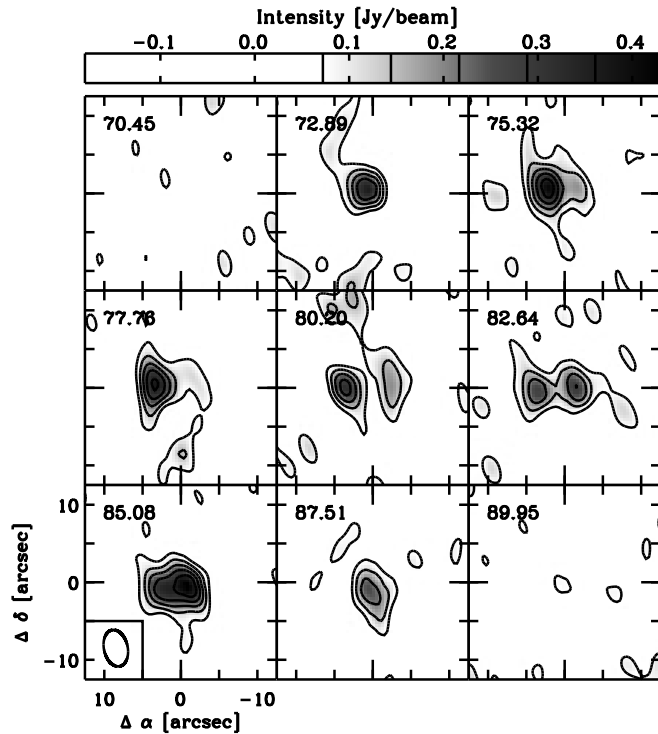


Fig. 3. Maps of the $^{12}\text{CO } J=1-0$ intensity for the LSR velocities indicated in the upper left corner of each box (contours: 72 (2σ), 144, 216, 288, and $360 \text{ mJy beam}^{-1}$). The spatial units are offsets in arcseconds with respect to the assumed position for the central star. Up is north and left is east. The Gaussian clean beam ($4.8'' \times 3.1''$ at a position angle of 13°) is inserted in the lower left map. In order to increase the signal to noise ratio in the maps we smoothed the channels to a velocity resolution of 2.4 km s^{-1} . The rms noise in the maps is about 36 mJy beam^{-1} .

velocity intervals of 2.4 km s^{-1} . At $v_{\text{SYS}} = 80.2 \text{ km s}^{-1}$ two intensity maxima west and east of the nucleus position, separated by about $6''$, are seen. At red-shifted velocities ($> 80.2 \text{ km s}^{-1}$) these two maxima are moving together and merge at the largest red-shifted velocities into one intensity peak. At blue-shifted velocities ($< 80.2 \text{ km s}^{-1}$) only one intensity maximum, east of the core position, is seen which gets closer to the center position with increasing blue-shifted velocities. This kinematical pattern can be explained by an expanding molecular torus, which is disrupted in its approaching, western side. Note that the front side (blue-shifted gas) of the torus lies to the north of the center and the back side (red-shifted gas) to the south.

To visualize in another way the kinematical structure, we show in Fig. 4 the right ascension-velocity diagram (top left) for a declination offset $\Delta\delta = 0''$ and the declination-velocity diagram (top right) for a right ascension offset $\Delta\alpha = 0''$, respectively.

The right ascension-velocity diagram reveals an elliptical structure, as we would expect for a toroidal distribution of the molecular gas. The two separated velocity components which are observed at the central position are joined up in one unique

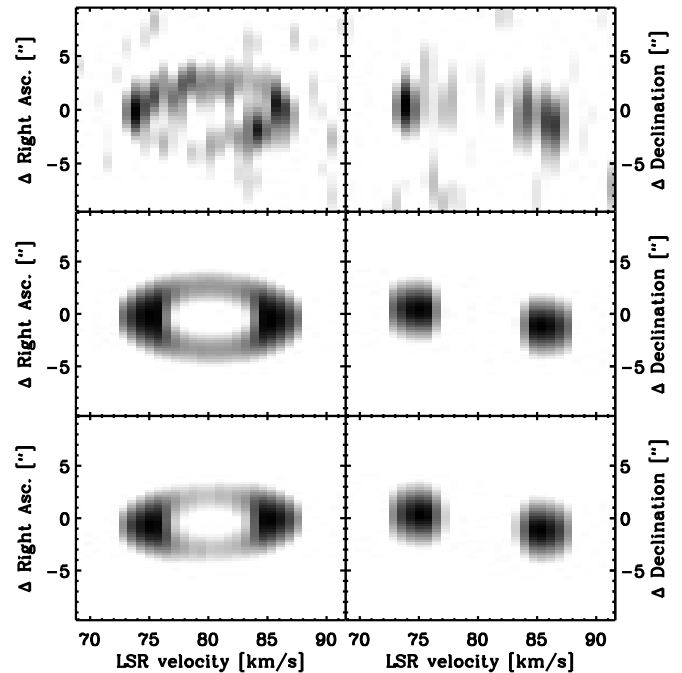


Fig. 4. Comparison of observed CO position-velocity diagrams with synthetic ones. First row: observed right ascension-velocity diagram for a declination offset of $\Delta\delta = 0''$ (left) and observed declination-velocity diagram for a right ascension offset of $\Delta\alpha = 0''$ (right). Second and third row: the corresponding position-velocity diagrams obtained from the non-rotating, circular and elliptical models (see text for details). Here, in contrast to Fig. 3 the velocity resolution is 0.8 km s^{-1} .

component that we observe on each side west and east of the nucleus. Again, one recognizes the disruption in the approaching, western side of the torus. The major axis of the elliptical structure in the right ascension-velocity diagram seems to be slightly tilted with respect to the horizontal.

The declination-velocity diagram shows the structure of the molecular gas along the north-south direction. The CO emission is found to be blue-shifted toward the north of the nucleus and red-shifted toward the south. The natural explanation for this effect is to assume that the torus is in expansion and tilted with respect to the line of sight.

From Fig. 4 we have estimated that the symmetry axis of the torus is inclined by about 17° with respect to the plane of the sky. For comparison, Goodrich (1991) and Schwarz et al. (1995) found from optical observations for the inclination angle of the nebular lobes with respect to the plane of the sky 11° and 22° , respectively. Optical spectroscopy also yielded that the southern lobe points towards us, in agreement with our observations.

The de-projected expansion velocity of the molecular gas is $\sim 7 \text{ km s}^{-1}$, a value which is relatively small when compared with expansion velocities of circumstellar envelopes of AGB-stars (Loup et al. 1993). For a mean radius of the torus of $3''$ we obtain a kinematical age of 2100 years assuming a distance of 1 kpc. It appears that the CO envelope of M 2-9 is

Table 1. Model parameters for the molecular envelope

Torus parameter	Circ. Model	Ell. Model
Major semi-axis a	3''	3''
Excentricity	—	0.55
Thickness r of the toroidal cylinder at a	2.2''	2.2''
Expansion velocity	7 km s ⁻¹	7 km s ⁻¹
Inclination angle	17°	17°
Angle of a with respect to the line of sight	—	20°

relatively young, and this explains why the CO molecules have not yet been totally photodissociated by the ultraviolet radiation from the central star. For a discussion of this point we refer to Bachiller et al. (1988).

3.3. Spatio-kinematic models for the molecular envelope

We have constructed spatio-kinematic models for the molecular envelope of M 2-9. We assumed, that the molecular gas is distributed in an expanding torus of constant density, which could be either circular or slightly elliptical. Assuming optically thin emission, a constant excitation in the CO line, an expansion velocity and a thickness r of the toroidal cylinder both proportional to the distance from the central star, we have calculated synthetic position-velocity diagrams. The results for an expanding, *circular* and an *elliptical* torus, respectively, which reproduce satisfactorily the observations are shown in the bottom two rows of Fig. 4. However, an expanding, *circular* torus which simultaneously rotates with a velocity of 1.5 km s⁻¹ around its symmetry axis (in such a manner that its western side is approaching us) gives a result similar to that of the elliptical model. The best fit parameters of the circular and the elliptical model obtained by reproducing the morphology and kinematics of the envelope are summarized in Table 1.

In spite of the crude assumption of optically thin emission, which leads to an overestimation of the intensity contrast between the different velocity components, the agreement of the models with the observations is satisfactory, at least qualitatively. We conclude, therefore, that a circular, non-rotating, clumpy torus can explain the observations to first order. However, the tilt of the ellipse in the right ascension-velocity diagram, only tentatively detected, is not unlikely, because: (a) an ellipticity of the torus can be expected if there are perturbations in the equatorial plane and (b) rotation is proposed by different authors (e.g. Dorfi and Hoefner 1996) in order to explain asymmetric mass loss from AGB-stars.

3.4. Molecular mass of the torus

In order to estimate the mass we first determined a lower limit for the total CO column density, using the integrated $J=1-0$ line intensity under the assumption of optically thin emission and LTE conditions. Assuming an excitation temperature of 25 K, we get a lower limit for the CO column density of $6.3 \cdot 10^{15} \text{ cm}^{-2}$.

This is comparable to the value of about 10^{15} cm^{-2} obtained by Bachiller et al. (1990) using transfer calculations in the large velocity gradient approximation. A lower limit for the mass of the molecular gas in the nebula can then be estimated by integrating the CO column density over the face of the molecular torus and by adopting a CO to H₂ abundance ratio. As the CO molecules are being photodissociated in the envelope, the present CO abundance is difficult to know. In particular there will be gradients in the CO abundance within the edges of the molecular clumps due to the penetration of ultraviolet photons from the central star. Bachiller et al. (1989) estimated in the case of NGC 2346, whose CO envelope age is similar to that of M 2-9, a CO/H₂ abundance ratio of $2 \cdot 10^{-5}$. Using this value we obtain for the molecular mass a lower limit of $9 \cdot 10^{-3} M_{\odot}$. The molecular mass could therefore be comparable to the ionized mass of the nebula, which is estimated to be about $10^{-2} M_{\odot}$ (Kwok et al. 1985).

4. Summary

The observed equatorial, expanding and clumpy CO torus around the waist of M 2-9 fits nicely in the evolutionary scheme for molecular envelopes of planetary nebulae described by Huggins et al. (1996). It is very likely formed by the dissociation and ionization of an originally neutral ellipsoidal shell, expelled during the AGB evolutionary stage. The destruction of the shell begins with the rapid dissociation and ionization of the least dense polar caps, and continues until the denser nebular waist is fully dissociated and ionized. The clumpiness of the molecular gas in M 2-9 gives further evidence to the fact that the medium in AGB- and post-AGB envelopes is clumpy at some scale. This is also suggested by several observations of molecular envelopes done in the last few years (see for that purpose the review by Olofsson 1996). The CO morphology of M 2-9 is similar to the disrupted, expanding molecular rings observed in the PNe NGC 2346, NGC 6720 and NGC 6772. However, the molecular mass in M 2-9 is at least one order of magnitude smaller than in those nebulae. This could be related to its lower luminosity and perhaps to a possible lower mass of the M 2-9 progenitor.

Our observations give strong support to the idea that M 2-9 is a young bipolar planetary nebula, whose nucleus is probably a binary. But further interferometric observations of high spatial resolution and signal to noise ratio, e.g. in the $^{12}\text{CO } J=2-1$ line, are needed to clarify the nature (ellipticity or rotation) of the tentatively detected tilt of the kinematical pattern in the right ascension-velocity diagram and the structure of the possibly binary nucleus.

Acknowledgements. We thank D. Morris and P.J. Huggins for the careful reading of the paper and their helpful suggestions. R.B. and V.B. acknowledge partial support from Spanish DGICYT through grant PB93-0048.

References

- Allen D.A., Swings J.P., 1972, ApJ 174, 583
Aspin C., McLean I.S., Smith M.G., 1988, A&A 196, 227

- Bachiller R., Gómez-González J., Bujarrabal V., Martin-Pintado J., 1988, A&A 196, L5
- Bachiller R., Planesas P., Martin-Pintado J., Bujarrabal V., Tafalla M., 1989, A&A 210, 366
- Bachiller R., Martin-Pintado J., Bujarrabal V., 1990, A&A 227, 188
- Balick B., 1987, AJ 94, 671
- Balick B., 1989, AJ 97, 476
- Dorfi E.A., Hoefner S., 1996, A&A 313, 605
- Feibelman W.A., 1984, ApJ 287, 353
- Goodrich R.W., 1991, ApJ 366, 163
- Guilloteau S., Delannoy J., Downes D., Greve A., Guélin M., Lucas R., Morris D., Radford S.J.E., Wink J., Cernicharo J., Forveille T., Garcia-Burillo S., Neri R., Blondel J., Perrigouard A., Plathner D., Torres M., 1992, A&A 262, 624
- Hoare M.G., Roche P.F., Clegg R.E.S., 1992, MNRAS 258, 257
- Huggins P.J., Bachiller R., Cox P., Forveille T., 1996, A&A 315, 284
- Kwok S., Purton C.R., Matthews H.E., Spoelstra T.A., 1985, A&A 144, 321
- Loup C., Forveille T., Omont A., Paul J., 1993, A&AS 99, 291
- Minkowski R., 1947, PASP 59, 257
- Morris M., 1981, ApJ 249, 572
- Olofsson H., 1996, preprint
- Phillips J.P., Mampaso A., 1988, A&A 190, 237
- Purton C.R., Feldman P.A., Marsh K.A., Allen D.A., Wright A.E., 1982, MNRAS 198, 321
- Schwarz H.E., Aspin C., Corradi R.L.M., Reiputh B., 1995, in Asymmetrical Planetary Nebulae, Annals of the Israel Physical Society, Vol.11, eds. Harpaz A. and Soker N., p.292
- Swings J.P., Andrillat Y., 1979, A&A 74, 85
- Zijlstra A.A., Pottasch S.R., Bignell C., 1989, A&AS 79, 329